

Coupled Triboelectric Nanogenerator Networks for Efficient Water Wave Energy Harvesting

Liang Xu,^{†,‡,§} Tao Jiang,^{†,‡,§} Pei Lin,^{†,‡,§} Jia Jia Shao,^{†,‡} Chuan He,^{†,‡} Wei Zhong,^{†,‡} Xiang Yu Chen,^{†,‡} and Zhong Lin Wang^{*,†,‡,§}

[†]Beijing Institute of Nanoenergy and Nanosystems, Chinese Academy of Sciences, Beijing 100083, P. R. China

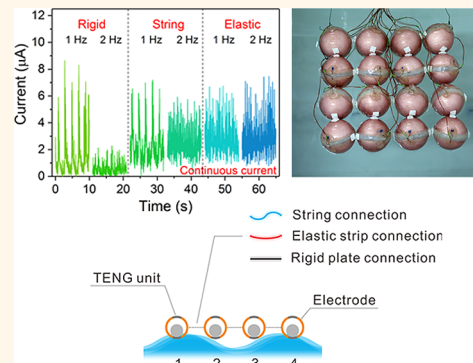
[‡]College of Nanoscience and Technology, University of Chinese Academy of Sciences, Beijing 100049, P. R. China

[§]School of Material Science and Engineering, Georgia Institute of Technology, Atlanta, Georgia 30332, United States

Supporting Information

ABSTRACT: Water wave energy is a promising clean energy source, which is abundant but hard to scavenge economically. Triboelectric nanogenerator (TENG) networks provide an effective approach toward massive harvesting of water wave energy in oceans. In this work, a coupling design in TENG networks for such purposes is reported. The charge output of the rationally linked units is over 10 times of that without linkage. TENG networks of three different connecting methods are fabricated and show better performance for the ones with flexible connections. The network is based on an optimized ball-shell structured TENG unit with high responsivity to small agitations. The dynamic behavior of single and multiple TENG units is also investigated comprehensively to fully understand their performance in water. The study shows that a rational design on the linkage among the units could be an effective strategy for TENG clusters to operate collaboratively for reaching a higher performance.

KEYWORDS: triboelectric nanogenerator networks, water wave energy harvesting, coupling behavior, ball-shell structure, blue energy



As threatened by climate change and resource crisis, developing renewable and clean energy has been a focused goal for the world.^{1–3} Water wave energy is a promising clean energy source that is especially abundant in the ocean. The power from waves around the coastlines worldwide was estimated to be over 2 TW (1 TW = 10^{12} W).^{4,5} Although having explored for decades, there still lack economical technologies to extract water wave energy at a large-scale.^{6–8} Current machines usually have complex hydraulic or mechanical structures to catch wave energy and convert it into rotary motion or linear reciprocal motion for driving an electromagnetic generator.^{9–11} Such designs make the whole device complicated, heavy, and costly. More importantly, the conversion efficiency is so low at low rotation frequency.¹²

The concept of using triboelectric nanogenerator (TENG) networks was first proposed by Wang in 2014, and it shows another route toward the goal to harness water wave energy.^{13,14} The TENG, as driven by the Maxwell's displacement current, can effectively convert mechanical energy into electricity based on the conjugation of tribo-electrification and electrostatic induction.^{15,16} Since its birth, TENGs with different structures have demonstrated versatile abilities to harvest mechanical energy from various sources especially at

low frequency, such as wind, human walking, infrastructure vibration, *etc.*^{12,17–22} Among various mechanical energy harvesting technologies, it has the merits of simple structure, large design flexibility, abundant choices of materials, and low cost.^{16,23–28} These features render the TENG networks to be a viable technology to catch water waves that are of low frequency.¹⁴ Several TENG prototypes have been fabricated and demonstrated effective harvesting of water wave energy.^{5,29–34} Nevertheless, the present works mainly focus on the structure and performance optimization of single devices, while the TENG network still remains to be experimented.

In this work, TENG networks based on an optimized ball-shell structured unit are reported. First, we demonstrate a TENG unit using treated silicone rubber as triboelectric materials, which gives a high output at small agitations. The dynamic behavior and angular dependence under harmonic and impact agitations are studied comprehensively to obtain a full

Received: December 7, 2017

Accepted: January 12, 2018

Published: January 12, 2018

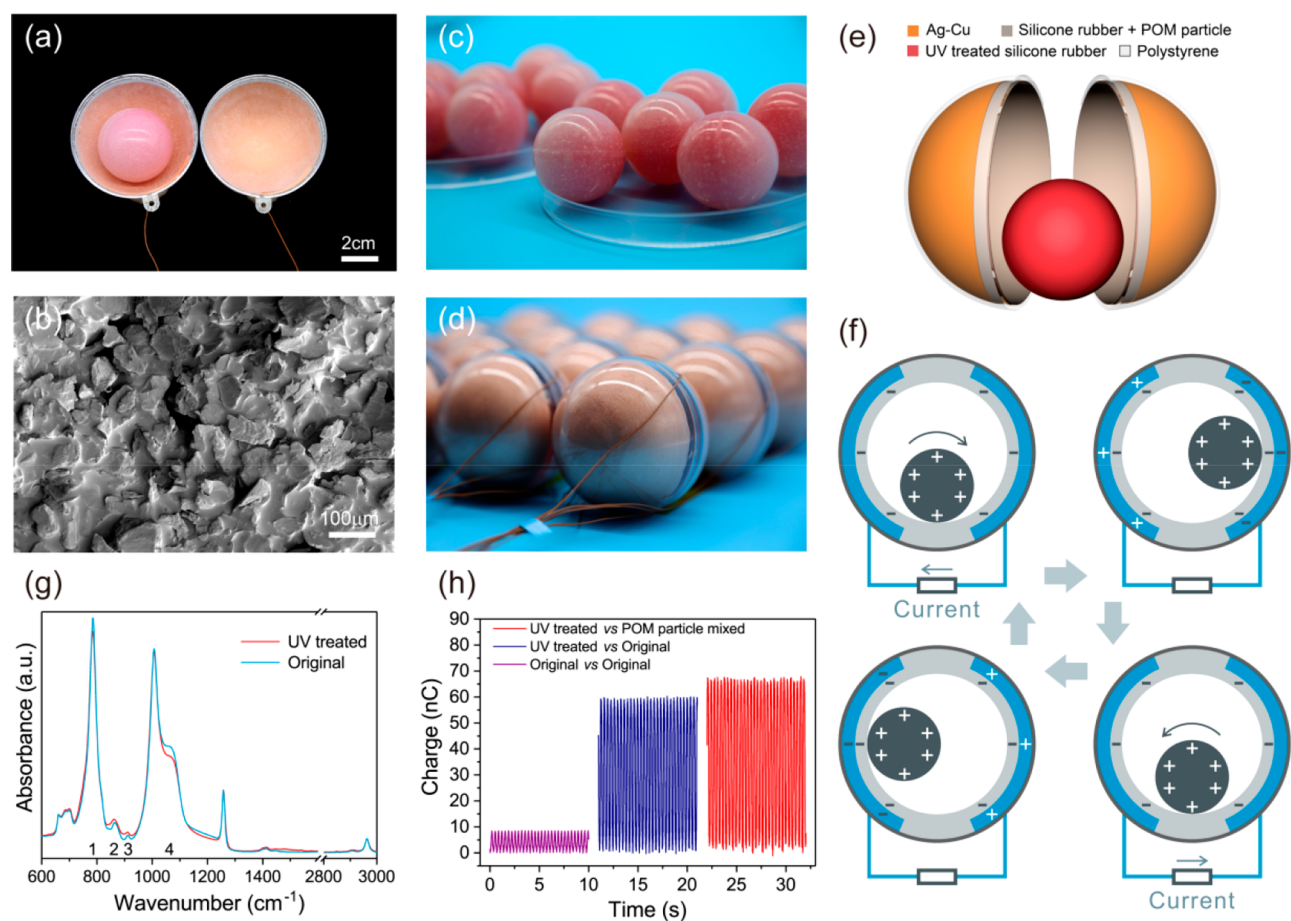


Figure 1. Structure and working principle of the TENG unit. (a, c, d) Photographs of a split ball-shell structured TENG unit, silicone rubber balls, and outer shells. (b) SEM image of silicone rubber mixed with POM particles. (e) Schematic structure of the TENG unit. (f) Working principle of the TENG unit. (g) FTIR spectra of the UV treated and the original balls. (h) Tribo-electrification performance for different pairs of the ball and the shell under the same harmonic agitation.

understanding of such kinds of TENG units. The aggregated performance of multiple TENG units is also investigated, and quasi-continuous direct current can be observed for groups of TENGs. Based on these, a coupling behavior for units linked with each other in TENG networks is presented. The charge output for rationally designed coupled units is over 10 times of that without coupling. TENG networks with three different connection methods were fabricated and characterized; the ones with flexible connections show higher efficiency. The coupled TENG network is an effective way to harvest water wave energy, which is a direction for future development for blue energy.

RESULTS AND DISCUSSION

Structure and Working Principle. A photograph of a split ball-shell structured TENG (BS-TENG) unit is shown in Figure 1a, and Figure 1e illustrates its detailed structure. The TENG unit consists of one ball and two semispherical shells with metal electrodes and dielectric layers on their inner surfaces. Figure 1c and d shows a group of fabricated balls and shells. Here, silicone rubber was used to prepare the ball and the dielectric layer, where its softness would enhance the real contact area and contribute to the durability of the device. Ultraviolet (UV) treatment was applied to the ball, which has a modification effect to the surface as shown in Figure 1g; the Fourier transform infrared (FTIR) spectra of the original and

the UV treated silicone rubber indicate decreased band intensity characteristic of the Si–O–Si signal (band 4 noted in the figure), accompanied by weakened Si–CH₃ signal (band 1) and enhanced Si–OH signals (bands 2 and 3) after the treatment, implying Si–O–Si chain scission and oxidative conversion of radical groups.³⁵ This seems to introduce a difference in the affinity to electrons for the ball and the dielectric layer, manifesting a strong tribo-electrification effect in the context of good surface contact (Figure 1h). To further enhance the contact electrification, polyformaldehyde (POM) particles were mixed into the dielectric layer, fabricating microstructures on the surface,^{36,37} as shown in Figure 1b (bare silicone rubber surface is shown in Figure S1 for comparison). The UV treatment and the microstructures also make the surface less sticky,³⁸ enabling smooth roll of the ball on the dielectric layer with relative low damping force, which is crucial for the performance of the TENG unit agitated by slow water waves. The electrodes were fabricated by painting commercial Ag–Cu conductive paint on the inner surface of the shell.

The operation mechanism of the BS-TENG unit is mainly based on the conjugation of tribo-electrification and electrostatic induction.¹⁷ As shown in Figure 1f, when the ball rolls in the spherical shell, the surfaces of the dielectric layer and the ball would be tribo-electrified, with static charges of the same amount and opposite signs. Accompanying the back and forth

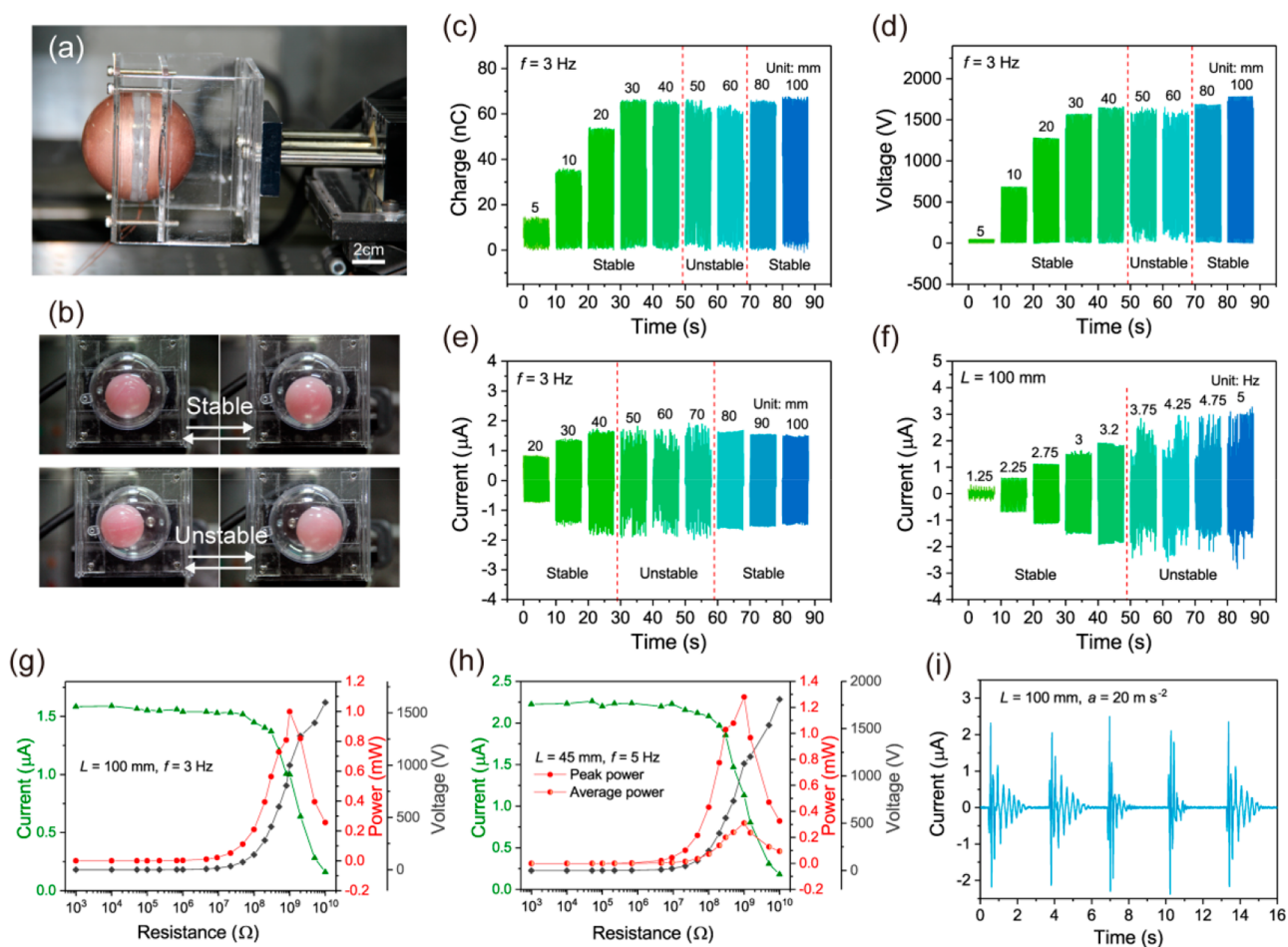


Figure 2. Electrical characterization of a single TENG unit by a motor in air. (a) Experiment setup for single TENG unit tests. (b) The stable and unstable motion of the ball in a shell without electrodes and dielectric layers. (c–e) Dependence of transferred charges, open circuit voltage, and short circuit current on the displacement amplitude of harmonic agitations. (f) Dependence of short circuit current on the frequency of harmonic agitations. (g, h) Dependence of the output power of the TENG unit on resistive loads for different harmonic agitations. (i) Short circuit current of the TENG unit for impact agitations with the acceleration $a = 20 \text{ m s}^{-2}$.

movement of the ball, the positive charges on its surface would induce negative charges to flow between the two electrodes on the shell through an external circuit, generating alternate current in the circuit. To stimulate the roll of the ball in the shell, various mechanical agitations can be adopted, like rotate or linearly shake the shell. Such mechanism of the device can be classified into the freestanding triboelectric layer mode,^{17,39} where the ball acts as the freestanding layer.

Characterization of a Single TENG Unit. To comprehensively understand the behavior of the BS-TENG under external mechanical excitations, a single unit was clamped in a chucking fixed on a linear motor that can impose harmonic and impact agitations to the unit in a translational mode, as shown in Figure 2a. Typical displacement curves of the agitations are presented in Figure S2 in the Supporting Information. First, we focus on the electrical outputs under various displacement amplitudes L and frequencies f for harmonic agitations. As shown in Figure 2c, for an agitation of 3 Hz, the short circuit transferred charges Q_{SC} increase rapidly with initial rise of the displacement amplitude, from 14 nC at 5 mm to 66 nC at 30 mm, then saturate with further increase of the amplitude. The open circuit voltage V_{OC} and the short circuit current I_{SC} show similar behavior, which can reach 1780 V and 1.8 μA , respectively, in the stable region (Figure 2d and e). Such

behavior indicates that the device can present high performance under subtle agitations, which is ideal for water wave energy harvesting. It can be observed that there exists a region around 50 mm to 60 mm, where the output waveform is chaotic. This can be attributed to the unstable motion of the ball as illustrated in Figure 2b and Videos S1 and S2 in the Supporting Information. Different from a stable motion where the ball simply rolls along the agitation direction, the ball in an unstable motion state would roll in a chaotic way, sometimes perpendicular to the agitation direction. The phenomenon should originate from the nonlinear dynamic nature of the ball-shell system that could show complex behavior under simple excitations. In such unstable motion state, the device would not have a strong dependence on the direction of the water wave, and whatever the agitation direction is, the ball could have movement along the direction between the two electrodes that can generate electricity effectively. The dependence of the short circuit current on the frequency was also investigated, as shown in Figure 2f. The current increases monotonically with the frequency and enters an unstable region after 3.2 Hz, where a maximum current of about 3 μA can be observed at 5 Hz.

The output power of the unit was measured with varying external resistance. The maximum peak power P_{peak} reaches 1 mW and 1.28 mW for agitations of 3 and 5 Hz, respectively,

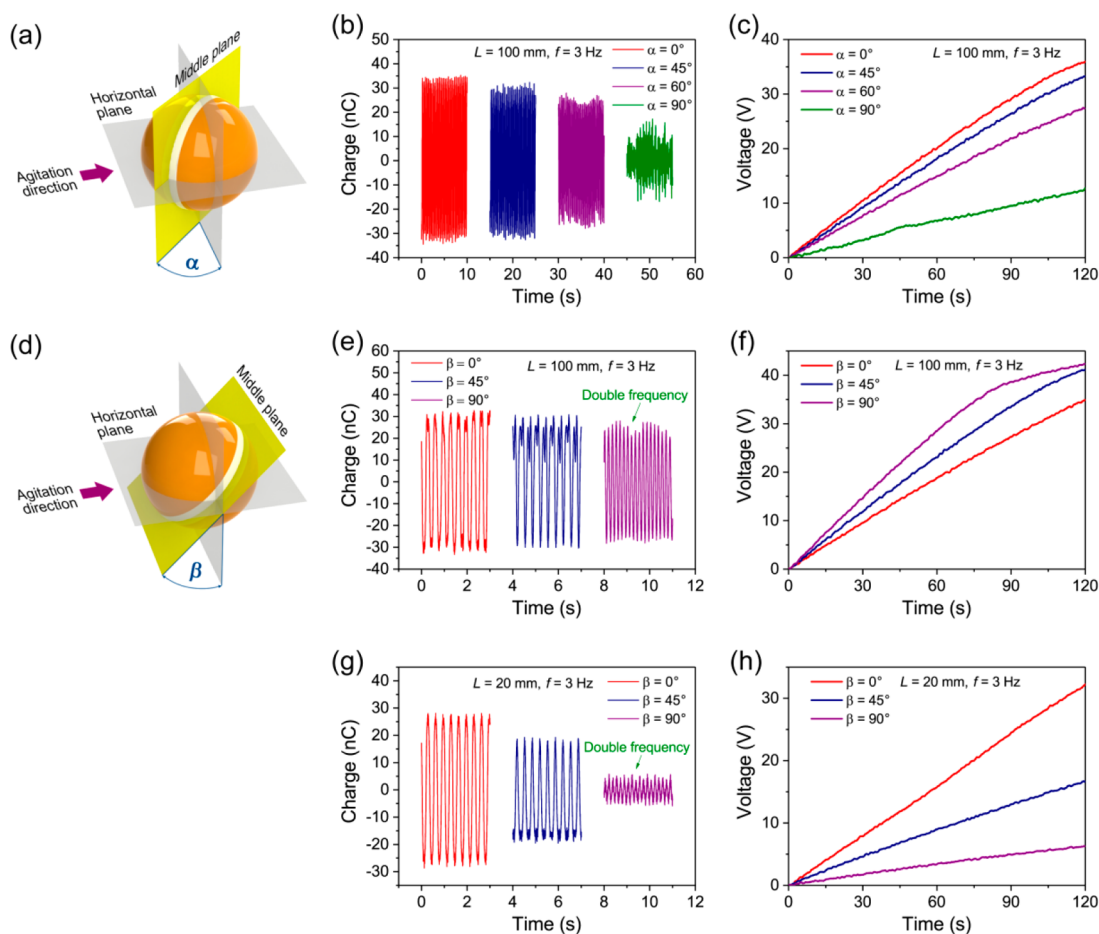


Figure 3. Orientation dependence of the output for a single TENG unit in air. (a, d) Schematic diagram of two orientation angles of the TENG unit. (b, e, g) Transferred charges of the TENG unit with different orientations. (c, f, h) Comparison of charging performance of the TENG unit to a capacitor of $1.07 \mu\text{F}$ with different orientations.

with matched resistance of around $1 \text{ G}\Omega$ (Figure 2g and h). The high matched resistance should originate from the low inherent capacitance of the device.^{28,40} We also calculated the average power P_{ave} for the 5 Hz case, using the following equation:^{28,40}

$$P_{\text{ave}} = \frac{\int_{t_0}^{t_0+T} I^2 R dt}{T} \quad (1)$$

where R represents the resistive load, I is the corresponding current, and T is the period of the current waveform. A maximum average power of 0.31 mW can be obtained with matched resistance, which is about 24% of the peak power. Here, the average power shows less decay relative to the peak power, since the TENG is in freestanding triboelectric mode where single current pulses have much longer duration compared to the vertical contact-separation mode.^{40,41}

Under impact agitations, a short circuit current of $2.4 \mu\text{A}$ can be obtained (Figure 2i), and the ball will oscillate to output about 10 pulses of current after single impacts. This shows that the device can store the mechanical energy and continuously translate it into electricity through internal vibrations afterward.

While in operation, the soft surface of the inner ball prohibits the ball from violently colliding with the shell. Thus, the device is expected to have excellent durability. A TENG unit tested for several days can still have very stable output without any decay

in our experiments, and an 1 h continuous test is shown in Figure S3 in the Supporting Information.

The exact matching between the water wave propagation direction and the electrode arrangement was considered important for the performance of such kind of devices, thus multiple electrodes were designed to harvest energy from different directions in previous works.²⁹ Nevertheless, we have shown above that for a two electrode design, unstable motion would still enable energy harvesting from water waves of random directions. Here, we will further discuss the angular dependence of the output performance in a stable motion. First, as shown in Figure 3a and d, we define a middle plane that lies in the middle between the two semispherical electrodes, and two orientation angles, that is, yaw angle α and pitch angle β , in reference to the agitation direction and the horizontal plane. It is easy to understand that there will be electrical output theoretically only when the movement of the ball have a nonzero projection in the direction perpendicular to the middle plane according to the proposed working principle in Figure 1f.

In the experiments, we first increased the yaw angle α from 0° to 90° and measured the transferred charges, as shown in Figure 3b. The transferred charges decrease slowly with larger angles. For a worst situation of 90° , where the device should have no output theoretically because the ball would roll along the middle plane, there is still an output of about 25 nC . This should be attributed to small asymmetries in the motion of the

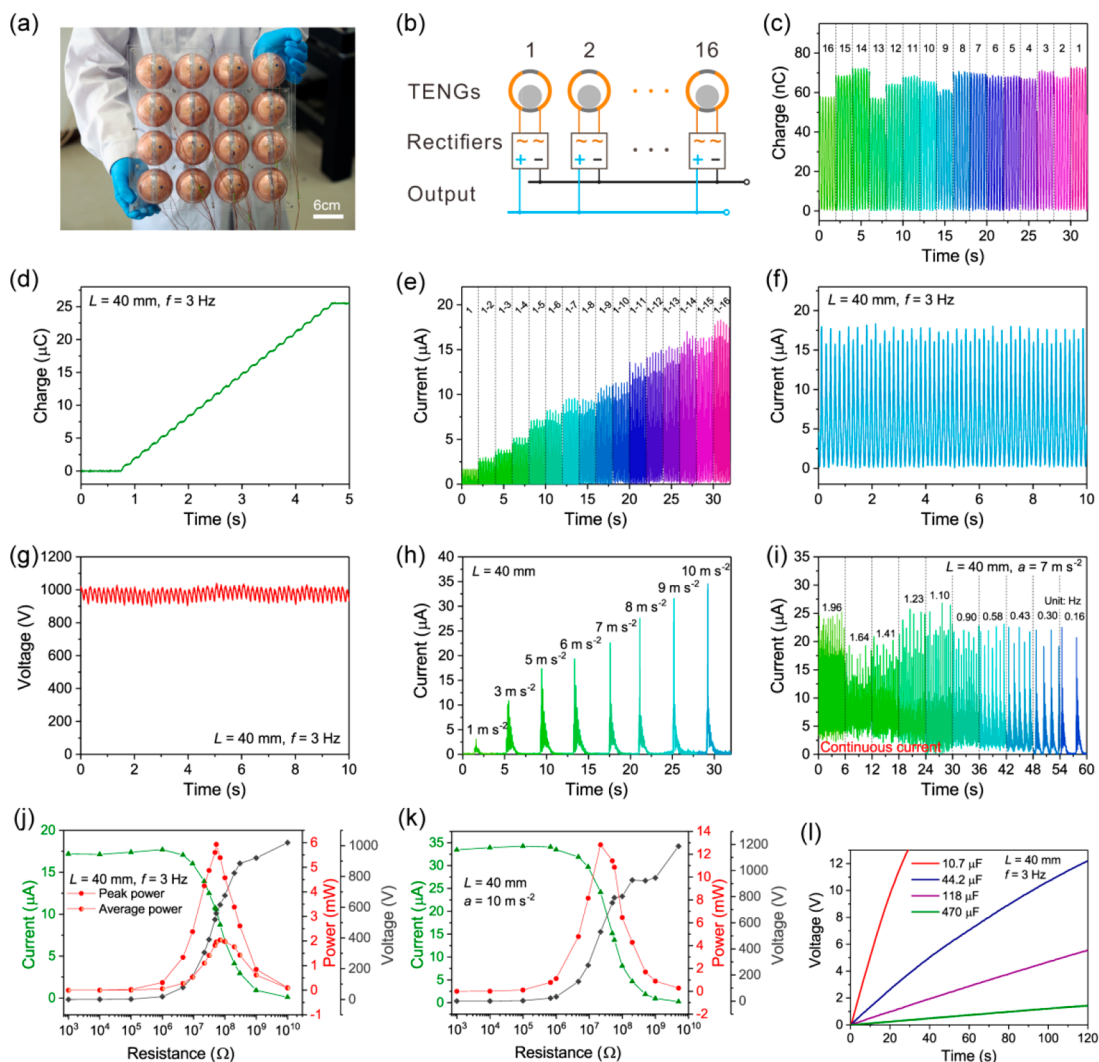


Figure 4. Electrical characterization of the 4×4 TENG array in air. (a) Photograph of the 4×4 TENG array. (b) Schematic diagram of the rectification circuit for the array. (c–g) Output of the TENG array for harmonic agitations with $L = 40$ mm and $f = 3$ Hz: (c) is transferred charges for each TENG unit in the array, (e) shows rectified short circuit current with different amounts of TENG units, and (d, f, g) show charge output, short circuit current, and open circuit voltage of the array with rectification. The TENG units are numbered as noted in (c) and (e). (h, i) Rectified short circuit current of the array under impact agitations of different accelerations and frequencies. (j, k) Dependence of the output power of the array on resistive loads for harmonic agitations and impact agitations, respectively. (l) Charging performance of the array for different capacitors with harmonic agitations.

ball to the middle plane and the sensitive response of the device to subtle agitations as shown in Figure 2c. We also charged a capacitor of $1.07 \mu\text{F}$ to get a reliable comparison of the accumulative output charges, which shows similar trend, and the charging rate is about 77% for 60° and 35% for 90° , as compared to the data at 0° (Figure 3c), indicating that the device with simple two-electrode design can have excellent energy harvesting performance for water waves from most directions.

For the pitch angle β , although the transferred charges reduce from 64 nC at 0° to 54 nC at 90° , the fluctuation frequency of charge output shows an unexpected doubling effect at 90° . As a result, the charging rate is even higher at 90° than at 0° (Figure 3e and f). This is due to the relative motion behavior of the ball to the electrodes; when the pitch angle is 90° , the middle plane would coincide with the horizontal plane, and the ball would have two chances to move back and forth to the upper electrode in a single roll cycle, producing two pulses of output. For a smaller amplitude of the drive motion, the

transferred charges would decrease much faster for 90° (Figure 3g), thus although there is still a double frequency effect, the charging rate at 90° is much lower than at 0° , as shown in Figure 3h. For the rest of the report, the yaw angle and the pitch angle are both set to 0° unless otherwise specified.

Characterization of a Rigid Network. For the application of water wave energy scavenging, TENG networks are required for large-scale energy harvesting.^{5,13,14} To understand the dependence of the output on the amount of TENG units and the performance of TENG groups, a 4×4 TENG array was fabricated, where the units were mechanically connected by rigid acrylic plates, as shown in Figure 4a. The electrical connection of the array is shown in Figure 4b. Considering it does not necessarily have the same phase, the output of each unit is rectified first, and all of them are connected in parallel.

The array was tested with harmonic agitations and impact agitations, respectively. We first tested the transferred charges of each unit without rectification under harmonic agitations, as shown in Figure 4c. The performance of each unit shows good

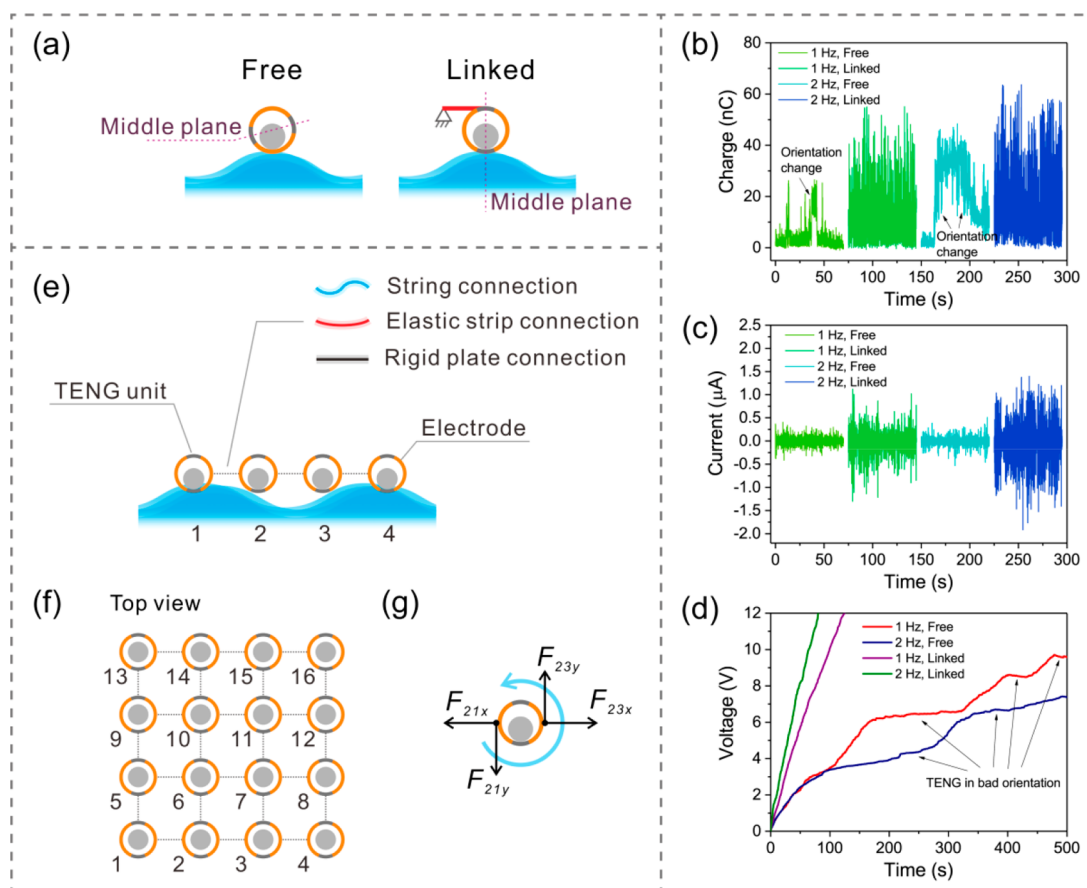


Figure 5. Schematic diagram and output comparison of mechanical connections for TENG units in water. (a) Schematic diagram of the experiment setup for a single TENG unit in water. (b, c) Transferred charges and short circuit current for the TENG unit in different states. (d) Charging performance to a capacitor of $1.07 \mu\text{F}$ for the TENG unit in different states. (e, f) Schematic diagram of network connecting strategies. (g) Force analysis for a TENG unit in the network.

uniformity, with an average value of 66.9 nC and a maximum of 72.6 nC , which is about 3 times as high as the highest value reported.²⁹ The rectified total transferred charges of 16 units for a single cycle $Q_{\text{SC},16}$ can be calculated as $2.138 \mu\text{C}$ from Figure 4d. The value is almost precisely the add-up of the output from each single unit in Figure 4c multiplying by a factor of 2 due to the rectification effect. The short circuit current shows a linear dependence on the amount of units, reaching $18.1 \mu\text{A}$ for 16 parallel connected units, as shown in Figure 4e and f. This is reasonable considering that the current is related to the rate of charge transfer:

$$I_{\text{SC},n} = \frac{dQ_{\text{SC},n}}{dt} \quad (2)$$

where $I_{\text{SC},n}$ and $Q_{\text{SC},n}$ represent short circuit current and transferred charges of n units, respectively. In the present array, the rigid connection makes the ball in each unit roll in roughly the same pace, thus with the linear increase of $Q_{\text{SC},n}$ by n , $I_{\text{SC},n}$ will also increase linearly. The measured open circuit voltage of the array $V_{\text{OC},16}$ is about 1020 V (Figure 4g), which is lower than the voltage of a single unit mentioned above. This could possibly be attributed to the adoption of the rectifier. The chip used here has a maximum blocking voltage of about 1000 V , thus it cannot reliably hold a higher voltage between the positive and the negative pins due to a rapid increasing reverse current in internal diodes with higher voltage. Because the open circuit state with a high voltage is not used for applications here,

we still use this rectifier in the research for its low cost and commercial availability.

The performance of the array under impact agitations is shown in Figure 4h and i. While the acceleration of agitations a increases, the peak short circuit current also rises almost linearly and achieves $34.5 \mu\text{A}$ with an acceleration of 10 m s^{-2} . For each current pulse, there is a long tail lasting about 1.8 s , where the current gradually decays to zero (Figure 4h). Due to such current tails, with shorter impact intervals, the current pulses corresponding to successive impacts would have influence with each other and finally present a continuous current of about $3 \mu\text{A}$ in addition to a fluctuating one, as shown in Figure 4i.

The output power for different resistive loads was measured under harmonic and impact agitations, respectively. For harmonic agitations, the measured data show a maximum peak power of 5.93 mW at $52.88 \text{ M}\Omega$ (Figure 4j), and a maximum average power of 2.04 mW (0.128 mW for each unit) can be obtained at $70.5 \text{ M}\Omega$ using Equation 1. The tiny discrepancy in the above optimum resistances could be attributed to that the average power is not just related to the peak point of the current as the peak power.⁴⁰ While considering the volume of the ball, the array produces a peak power density of about 2.06 W m^{-3} and an average power density of about 0.71 W m^{-3} . If the network covers a water area of 1 km^2 and extends into 5 m in depth of water, with each unit spaced about 7.5 cm , a maximum average power of 1.51 MW is expected to be delivered.

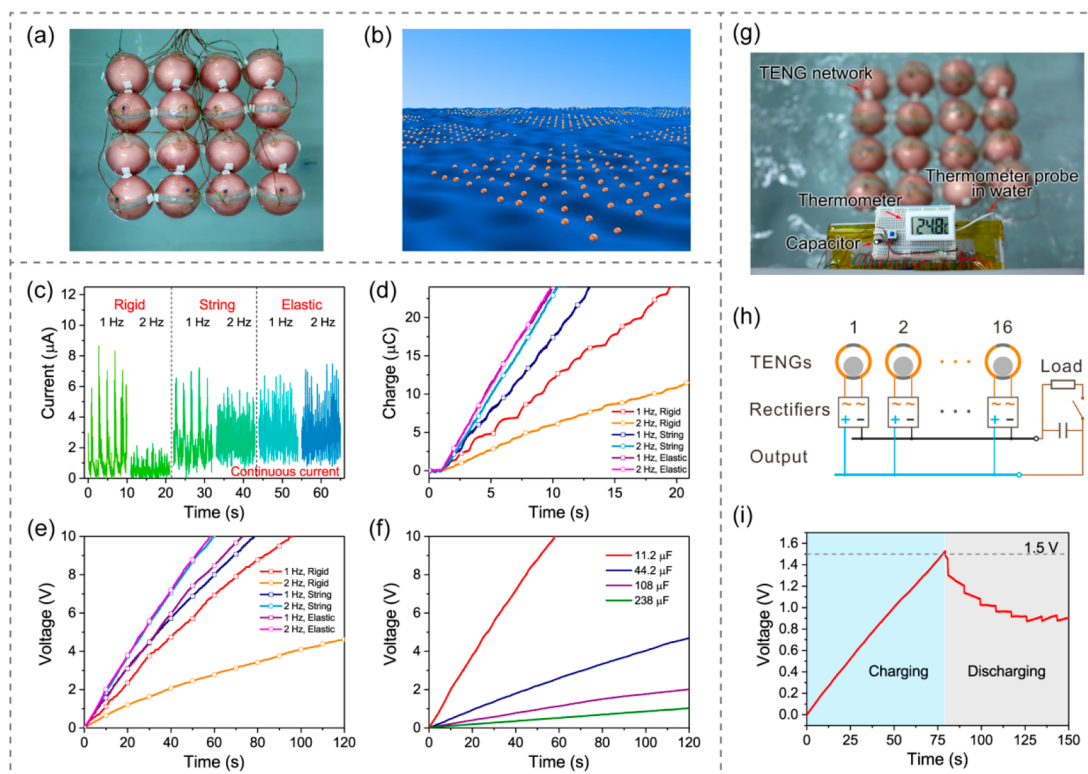


Figure 6. Comparison of the TENG networks with three different types of connecting strategies in water. (a) Photograph of the string connected TENG network. (b) Imaginary picture of future large-scale TENG networks for harvesting water wave blue energy. (c, d) Rectified short circuit current and transferred charges of three different types of TENG networks. (e) Charging performance of the three types of networks to a capacitor of $11.2 \mu\text{F}$. (f) Charging performance of the elastic strip connected network to different capacitors under water waves of 2 Hz. (g) Photograph of the string connected network to power a thermometer. (h) Schematic diagram of the circuit for powering the thermometer. (i) Charging and discharging processes for a capacitor of $108 \mu\text{F}$ to power the thermometer.

For impact agitations, as shown in Figure 4k, the measured data show a maximum peak power of 12.83 mW, with corresponding peak power density of 4.47 W m^{-3} .

To test the performance of the array for capacitive load, different capacitors were charged with the array, as shown in Figure 4l. Typically, the BS-TENG array can charge a capacitor of $44.2 \mu\text{F}$ to 3 V within 22.9 s, and the stored energy can be used to power small electronics, like thermometers, anemometers, etc.

Coupled TENG Networks in Water. The TENG network is proposed to harvest water wave energy in a large area.^{5,13,14} However, it is still not clear how the network should be organized to receive the maximum output power, and what is the function of the networking besides harvesting energy from distributed local sites. In this section, we investigate TENG arrays in real water circumstances and show a coupling behavior between TENG units by networking, which acts as a crucial role for TENGs to operate effectively in water waves.

In the study, wave tank experiments were carried out to test single TENG units and 4×4 TENG arrays with different network connection methods. The setup of the wave tank is shown in Figure S4 in the Supporting Information. First, as illustrated in Figure 5a, two sorts of TENG units were tested, referred to as the free-unit and the linked-unit. For the free-unit, the TENG floats freely on water surface, mimicking the unit in an array with no mechanical connections. For the linked-unit, the TENG is connected to a fixed pole above the water surface by a polycarbonate (PC) strip of 1 cm width and

0.3 cm thickness, mimicking units with certain mechanical coupling to a network.

The transferred charges of such units are shown in Figure 5b. For the free TENG unit, obvious drifts of the baseline of charge output can be observed, which reflect that the inner ball rolls to certain sites without completely rolling back due to orientation changes of the whole unit. Without effective constraints of a linkage, the orientation of the unit would vary arbitrarily, sometimes in a “dead” state where there is almost no output (Video S3 in the Supporting Information). Even in good orientations, the transferred charges can only reach about 30 nC for 2 Hz water waves. For the linked-unit, the performance improves significantly, with transferred charges of 63 nC and 55 nC in 2 and 1 Hz water waves, respectively, and the drift of the baseline is suppressed. The comparison shows the crucial roles played by the linkage that couples TENG units for proper operation in water. Two effects can be concluded: First, the constraint effect of the linkage helps the unit to maintain an optimum orientation as discussed above; and second, the linkage would transfer force and energy between units and impose a torque to the unit accompanied by the push of water waves, which drives the unit to rotate and to be excited effectively by slow water motion. The second effect can explain why even both in good orientations, the output improves substantially for the unit in the linked state versus that in the free state. The short circuit current shown in Figure 5c further confirms the role played by the linkage. We also tested charging performance of the units to a capacitor of $1.07 \mu\text{F}$, to show the long-term charge output and suppress short-term randomness

(Figure 5d). Charging curves for the free-unit show obvious plateaus where the voltage of the capacitor hardly has any increase for a long time. For the linked-unit, the charging is much faster, improving to about 11.6 times for 2 Hz water waves, to charge the capacitor to 7.5 V.

The above data indicate that the effects of proper linkage are musts for such TENG units to operate in water. For a group of TENGs, the harvesting efficiency could be very low as dispersed units covering large areas without linkage. Thus, mechanical connections between units in the TENG networks to effectively couple each unit play crucial roles. In the networks, each unit is mechanically linked to other units, so that the correlative mechanical movement by coupling among them gives a high output. To further illustrate the idea and test different connections, networks with three types of connections were proposed, that is, rigid plate connection which will not deform, elastic strip connection that can deform to some extent, and string connection that can freely deform without extension, as shown in Figure 5e. The connection topology is shown in Figure 5f. Details of the connection methods can be found in the Experimental Section. Figure 5g further clarifies the effects from unit coupling, using one-dimensional string connection as an example. In general, the connection can maintain the unit in a proper orientation, and meanwhile the force components at the link points, F_{21y} and F_{23y} , would impose a torque to the unit, along with the interaction force from the water, making the unit rotate or vibrate.

To test their performance in water, the above three types of networks were fabricated and tested in the wave tank with simulated water waves of frequencies 1 and 2 Hz, respectively (Figure 6a). As shown in Figure 6c, for the rigid connection, it can reach a rectified short circuit current of $8.3 \mu\text{A}$ at 1 Hz and $2.2 \mu\text{A}$ at 2 Hz. The rigid connection provides a strong constraint for the units in the network, which makes them move in a synchronized mode, resulting in relative large current peaks at 1 Hz. For 2 Hz, the wavelength and vibration amplitude reduce dramatically, and the output decreases rapidly (Video S4 in the Supporting Information). For the cases with the string connection and the elastic strip connection, which can be regarded as flexible connections, the networks perform well at both 1 and 2 Hz, and an internal vibration behavior between units can be observed, as shown in Video S5 in the Supporting Information. Their current signals have similar features that are composed by a continuous part of about $1 \mu\text{A}$ and a fluctuating part, with total current peaks ranging from $6 \mu\text{A}$ to $7.5 \mu\text{A}$. The rectified charge outputs are shown in Figure 6d, the elastic strip connection at 2 Hz shows the highest output rate of $2.7 \mu\text{C}$ every second. For each unit in such network, the charge output is about 10.8 times as that for free units shown in Figure 5a. To observe charge outputs in longer time scale and suppress possible randomness, a capacitor of $11.2 \mu\text{F}$ was charged with these networks, as shown in Figure 6e. The two flexible connections have similar performance for the same water wave frequency, with the cases at 2 Hz a bit higher than at 1 Hz. The rigid connection shows weaker output at 1 Hz and the worst result at 2 Hz. The above experiments indicate that flexible connections are better networking strategies than the rigid one which imposes too much internal constraints between units.

With excellent performance in water, the flexible networks can charge different capacitors efficiently (Figure 6f), capable of powering various small electronic devices, like sensors, wireless transmission modules, etc. Here, we demonstrate an application

for the network to supply electricity for a thermometer to measure the temperature of the water. The electrical circuit is shown in Figure 6h. The output of each unit is rectified and then parallel connected together to charge a capacitor of $108 \mu\text{F}$. After the voltage rose to about 1.5 V, the switch was closed, and the thermometer started to work to display the right temperature of the water, as shown in Figure 6g and Video S6 in the Supporting Information. The initial charging process took only about 78 s at 2 Hz using the string connected network (Figure 6i). A more profound idea is to harvest water wave energy from large areas with scaled up TENG networks, that is, blue energy,^{5,13,14} as shown in Figure 6b. With coupling between units, the TENG network is proved to be an effective way to harvest water wave energy. The aggregated power of units in large areas can be huge. Such electricity can be transferred to the grid on land or to small islands through submarine cables, providing an inexhaustible clean energy source for humans.

CONCLUSIONS

In summary, coupled TENG networks based on optimized BS-TENG units for water wave energy harvesting are reported. A rational design on the coupling among units greatly enhances the operating efficiency of the network. The charge output of the coupled units is over 10 times of that without coupling. TENG networks of three different connection methods were fabricated and characterized, with flexible connections performing much better than the rigid one for extra internal degrees of freedom. The unit of the TENG network adopts a typical ball-shell structure with optimized designs that have high responsiveness to small agitations. The dynamic behavior and angular dependence under harmonic and impact agitations are studied comprehensively to obtain a full understanding of such kind of TENG units. The aggregated performance of multiple TENGs is also investigated, and a quasi-continuous direct current can be observed for groups of TENGs. The report demonstrates that the coupled TENG network is an effective way to harvest water wave energy, toward the blue energy dream.

EXPERIMENTAL SECTION

Fabrication of the TENG Unit. For the inner ball, the base and the curing agent of the silicone rubber (PS6605) were mixed uniformly by volume ratio 1:1 and then poured into a ball-shaped mold with inner diameter of 4 cm. A hollow plastic ball of 3 cm was placed in the center of the mold to be wrapped up by the silicone rubber. After curing for 1 h at the temperature of 60°C , a hollow silicone rubber ball was prepared. The ball was then UV treated for 10 min using an UV cleaner (BZS250GF-TC). For the outer shell, Ag-Cu conductive paint (Changyuan 6330) was painted on the inner surface of the shell which has a diameter of 7 cm and baked at the temperature of 60°C for 0.5 h to form a tough layer of metal electrode. The silicone rubber (PS6605) was then smeared over the electrode with POM particles sprayed on and cured for 1 h at the temperature of 60°C .

Fabrication of the Network. For the rigid plate connected network, the 16 TENG units were placed between two acrylic plates which have 16 round holes with a diameter of 6.3 cm in a 4×4 array, and the TENG units were seated firmly in the holes. For the elastic strip connected network, plastic strips with a width of 1 cm were glued on every two neighboring TENG units to form a 4×4 arranged TENG array, according to the topology shown in Figure 5f. For the string connected network, every two neighboring TENG units in the array were bunched with strings by a distance of about 1 cm.

Electrical Characterization. The open circuit voltage was measured by an electrostatic voltmeter (Trek 344). The transferred

charges and the current were measured by an electrometer (Keithley 6514).

ASSOCIATED CONTENT

Supporting Information

The Supporting Information is available free of charge on the ACS Publications website at DOI: 10.1021/acsnano.7b08674.

SEM images of bare silicone rubber surface; typical displacement curves for agitation movement of the motor; transferred charges of the TENG unit under long-time operation; setup for wave tank experiments (PDF)
Video S1: Stable motion of the ball in a shell without electrodes and dielectric layers (AVI)

Video S2: Unstable motion of the ball in a shell without electrodes and dielectric layers (AVI)

Video S3: Free TENG unit under water waves of 2 Hz (AVI)

Video S4: Rigid network under water waves of 2 Hz (AVI)

Video S5: String connected network under water waves of 2 Hz (AVI)

Video S6: Powering a thermometer by the string connected network (AVI)

AUTHOR INFORMATION

Corresponding Author

*E-mail: zlwang@binn.cas.cn.

ORCID

Zhong Lin Wang: 0000-0002-5530-0380

Author Contributions

[#]These authors contributed equally to this work. L. Xu and Z. L. Wang conceived the idea, analyzed the data, and prepared the paper. L. Xu, T. Jiang, P. Lin, and W. Zhong fabricated the device. L. Xu, P. Lin, and C. He did the experiments. T. Jiang helped in the FEM calculation. J. J. Shao helped in the FTIR characterization and analysis. X. Y. Chen helped in improving the material. Z. L. Wang guided the whole project.

Notes

The authors declare no competing financial interest.

ACKNOWLEDGMENTS

We thank Chao Ran Deng for helping render the pictures of three-dimensional model. Research was supported by the National Key R & D Project from Minister of Science and Technology, China (2016YFA0202704), National Natural Science Foundation of China (grant nos. 51605033, 51432005, 5151101243, and 51561145021), the “Thousands Talents” Program for Pioneer Researcher and His Innovation Team, China, China Postdoctoral Science Foundation (grant no. 2015M581041), and Beijing Municipal Science & Technology Commission (grant no. Z171100000317001).

REFERENCES

- (1) Schiermeier, Q.; Tollefson, J.; Scully, T.; Witze, A.; Morton, O. Electricity without Carbon. *Nature* **2008**, *454*, 816–823.
- (2) Gielen, D.; Boshell, F.; Saygin, D. Climate and Energy Challenges for Materials Science. *Nat. Mater.* **2016**, *15*, 117–120.
- (3) Jacobson, M. Z.; Delucchi, M. A.; Bazouin, G.; Bauer, Z. A. F.; Heavey, C. C.; Fisher, E.; Morris, S. B.; Piekutowski, D. J. Y.; Vencill, T. A.; Yeskoo, T. W. 100% Clean and Renewable Wind, Water, and Sunlight (WWS) All-Sector Energy Roadmaps for the 50 United States. *Energy Environ. Sci.* **2015**, *8*, 2093–2117.

(4) Khaligh, A.; Onar, O. C. *Energy Harvesting: Solar, Wind, and Ocean Energy Conversion Systems*; CRC Press: Boca Raton, 2009; pp 223–225.

(5) Wang, Z. L.; Jiang, T.; Xu, L. Toward the Blue Energy Dream by Triboelectric Nanogenerator Networks. *Nano Energy* **2017**, *39*, 9–23.

(6) Salter, S. H. Wave Power. *Nature* **1974**, *249*, 720–724.

(7) Falcao, A. F. D. Wave Energy Utilization: A Review of the Technologies. *Renewable Sustainable Energy Rev.* **2010**, *14*, 899–918.

(8) Drew, B.; Plummer, A. R.; Sahinkaya, M. N. A Review of Wave Energy Converter Technology. *Proc. Inst. Mech. Eng., Part A* **2009**, *223*, 887–902.

(9) Tollefson, J. Power from the Oceans: Blue Energy. *Nature* **2014**, *508*, 302–304.

(10) Callaway, E. Energy: To Catch a Wave. *Nature* **2007**, *450*, 156–159.

(11) Scruggs, J.; Jacob, P. Engineering. Harvesting Ocean Wave Energy. *Science* **2009**, *323*, 1176–1178.

(12) Zi, Y. L.; Guo, H. Y.; Wen, Z.; Yeh, M. H.; Hu, C. G.; Wang, Z. L. Harvesting Low-Frequency (< 5 Hz) Irregular Mechanical Energy: A Possible Killer Application of Triboelectric Nanogenerator. *ACS Nano* **2016**, *10*, 4797–4805.

(13) Wang, Z. L. Triboelectric Nanogenerators as New Energy Technology and Self-Powered Sensors - Principles, Problems and Perspectives. *Faraday Discuss.* **2014**, *176*, 447–458.

(14) Wang, Z. L. Catch Wave Power in Floating Nets. *Nature* **2017**, *542*, 159–160.

(15) Fan, F. R.; Tian, Z. Q.; Wang, Z. L. Flexible Triboelectric Generator! *Nano Energy* **2012**, *1*, 328–334.

(16) Wang, Z. L. On Maxwell's Displacement Current for Energy and Sensors: the Origin of Nanogenerators. *Mater. Today* **2017**, *20*, 74–82.

(17) Wang, Z. L.; Chen, J.; Lin, L. Progress in Triboelectric Nanogenerators as a New Energy Technology and Self-Powered Sensors. *Energy Environ. Sci.* **2015**, *8*, 2250–2282.

(18) Zhu, G.; Peng, B.; Chen, J.; Jing, Q. S.; Wang, Z. L. Triboelectric Nanogenerators as a New Energy Technology: From Fundamentals, Devices, to Applications. *Nano Energy* **2015**, *14*, 126–138.

(19) Niu, S. M.; Wang, X. F.; Yi, F.; Zhou, Y. S.; Wang, Z. L. A Universal Self-Charging System Driven by Random Biomechanical Energy for Sustainable Operation of Mobile Electronics. *Nat. Commun.* **2015**, *6*, 8975.

(20) Zhu, G.; Zhou, Y. S.; Bai, P.; Meng, X. S.; Jing, Q. S.; Chen, J.; Wang, Z. L. A Shape-Adaptive Thin-Film-Based Approach for 50% High-Efficiency Energy Generation Through Micro-Grating Sliding Electrification. *Adv. Mater.* **2014**, *26*, 3788–3796.

(21) Zhu, G.; Su, Y. J.; Bai, P.; Chen, J.; Jing, Q. S.; Yang, W. Q.; Wang, Z. L. Harvesting Water Wave Energy by Asymmetric Screening of Electrostatic Charges on a Nanostructured Hydrophobic Thin-Film Surface. *ACS Nano* **2014**, *8*, 6031–6037.

(22) Wang, J.; Li, S. M.; Yi, F.; Zi, Y. L.; Lin, J.; Wang, X. F.; Xu, Y. L.; Wang, Z. L. Sustainably Powering Wearable Electronics Solely by Biomechanical Energy. *Nat. Commun.* **2016**, *7*, 12744.

(23) Wang, Z. L.; Song, J. H. Piezoelectric Nanogenerators Based on Zinc Oxide Nanowire Arrays. *Science* **2006**, *312*, 242–246.

(24) Dagdeviren, C.; Joe, P.; Tuzman, O. L.; Park, K.; Lee, K. J.; Shi, Y.; Huang, Y. G.; Rogers, J. A. Recent Progress in Flexible and Stretchable Piezoelectric Devices for Mechanical Energy Harvesting, Sensing and Actuation. *Extreme Mech. Lett.* **2016**, *9*, 269–281.

(25) El-hami, M.; Glynn-Jones, P.; White, N. M.; Hill, M.; Beeby, S.; James, E.; Brown, A. D.; Ross, J. N. Design and Fabrication of a New Vibration-Based Electromechanical Power Generator. *Sens. Actuators, A* **2001**, *92*, 335–342.

(26) Wang, H. S.; Jeong, C. K.; Seo, M. H.; Joe, D. J.; Han, J. H.; Yoon, J. B.; Lee, K. J. Performance-Enhanced Triboelectric Nanogenerator Enabled by Wafer-Scale Nanogrates of Multistep Pattern Downscaling. *Nano Energy* **2017**, *35*, 415–423.

(27) Zhang, C.; Tang, W.; Han, C. B.; Fan, F. R.; Wang, Z. L. Theoretical Comparison, Equivalent Transformation, and Conjunction Operations of Electromagnetic Induction Generator and Triboelectric

Nanogenerator for Harvesting Mechanical Energy. *Adv. Mater.* **2014**, *26*, 3580–3591.

(28) Niu, S. M.; Wang, Z. L. Theoretical Systems of Triboelectric Nanogenerators. *Nano Energy* **2015**, *14*, 161–192.

(29) Wang, X. F.; Niu, S. M.; Yin, Y. J.; Yi, F.; You, Z.; Wang, Z. L. Triboelectric Nanogenerator Based on Fully Enclosed Rolling Spherical Structure for Harvesting Low-Frequency Water Wave Energy. *Adv. Energy Mater.* **2015**, *5*, 1501467.

(30) Chen, J.; Yang, J.; Li, Z. L.; Fan, X.; Zi, Y. L.; Jing, Q. S.; Guo, H. Y.; Wen, Z.; Pradel, K. C.; Niu, S. M.; Wang, Z. L. Networks of Triboelectric Nanogenerators for Harvesting Water Wave Energy: A Potential Approach toward Blue Energy. *ACS Nano* **2015**, *9*, 3324–3331.

(31) Yang, Y.; Zhang, H. L.; Liu, R. Y.; Wen, X. N.; Hou, T. C.; Wang, Z. L. Fully Enclosed Triboelectric Nanogenerators for Applications in Water and Harsh Environments. *Adv. Energy Mater.* **2013**, *3*, 1563–1568.

(32) Zhang, L. M.; Han, C. B.; Jiang, T.; Zhou, T.; Li, X. H.; Zhang, C.; Wang, Z. L. Multilayer Wavy-Structured Robust Triboelectric Nanogenerator for Harvesting Water Wave Energy. *Nano Energy* **2016**, *22*, 87–94.

(33) Xu, L.; Pang, Y. K.; Zhang, C.; Jiang, T.; Chen, X. Y.; Luo, J. J.; Tang, W.; Cao, X.; Wang, Z. L. Integrated Triboelectric Nanogenerator Array Based on Air-Driven Membrane Structures for Water Wave Energy Harvesting. *Nano Energy* **2017**, *31*, 351–358.

(34) Wen, Z.; Guo, H.; Zi, Y.; Yeh, M. H.; Wang, X.; Deng, J.; Wang, J.; Li, S.; Hu, C.; Zhu, L.; Wang, Z. L. Harvesting Broad Frequency Band Blue Energy by a Triboelectric-Electromagnetic Hybrid Nanogenerator. *ACS Nano* **2016**, *10*, 6526–6534.

(35) Efimenko, K.; Wallace, W. E.; Genzer, J. Surface Modification of Sylgard-184 Poly(dimethyl siloxane) Networks by Ultraviolet and Ultraviolet/Ozone Treatment. *J. Colloid Interface Sci.* **2002**, *254*, 306–315.

(36) Yang, Y.; Zhang, H. L.; Chen, J.; Lee, S. M.; Hou, T. C.; Wang, Z. L. Simultaneously Harvesting Mechanical and Chemical Energies by a Hybrid Cell for Self-Powered Biosensors and Personal Electronics. *Energy Environ. Sci.* **2013**, *6*, 1744–1749.

(37) Li, H. Y.; Su, L.; Kuang, S. Y.; Pan, C. F.; Zhu, G.; Wang, Z. L. Significant Enhancement of Triboelectric Charge Density by Fluorinated Surface Modification in Nanoscale for Converting Mechanical Energy. *Adv. Funct. Mater.* **2015**, *25*, 5691–5697.

(38) Li, S. M.; Peng, W. B.; Wang, J.; Lin, L.; Zi, Y. L.; Zhang, G.; Wang, Z. L. All-Elastomer-Based Triboelectric Nanogenerator as a Keyboard Cover To Harvest Typing Energy. *ACS Nano* **2016**, *10*, 7973–7981.

(39) Wang, S. H.; Xie, Y. N.; Niu, S. M.; Lin, L.; Wang, Z. L. Freestanding Triboelectric-Layer-Based Nanogenerators for Harvesting Energy from a Moving Object or Human Motion in Contact and Non-contact Modes. *Adv. Mater.* **2014**, *26*, 2818–2824.

(40) Niu, S. M.; Liu, Y.; Chen, X. Y.; Wang, S. H.; Zhou, Y. S.; Lin, L.; Xie, Y. N.; Wang, Z. L. Theory of Freestanding Triboelectric-Layer-Based Nanogenerators. *Nano Energy* **2015**, *12*, 760–774.

(41) Niu, S. M.; Wang, S. H.; Lin, L.; Liu, Y.; Zhou, Y. S.; Hu, Y. F.; Wang, Z. L. Theoretical Study of Contact-Mode Triboelectric Nanogenerators as an Effective Power Source. *Energy Environ. Sci.* **2013**, *6*, 3576–3583.